

SAMPLE ALIGNMENT IN NEUTRON SCATTERING EXPERIMENTS USING DEEP NEURAL NETWORK

A. Diaw *, K. Bruhwiler, J. P. Edelen, C. C. Hall, RadiaSoft LLC, Boulder, CO
 S. Calder, C. Hoffmann, Oak Ridge National Laboratory, Oak Ridge, TN

Abstract

Neutron scattering facilities, such as Oak Ridge National Laboratory (ORNL) and the NIST Center for Neutron Research, provide a source of neutrons to investigate a wide variety of scientific and technologically relevant areas, including material science, chemistry, biology, physics, and engineering. In these experiments, the quality of the data collected is sensitive to sample and beam alignment. This alignment changes both between different samples and during measurements. The sample alignment optimization process requires human intervention to tune the beam and sample positions. While this procedure works, it is inefficient, time-consuming, and often not optimized to high precision alignment. This paper uses different neural network architectures on neutron camera images from the HB-2A powder diffractometer beamline at the High flux Isotope Reactor (HFIR) and optical camera images from the TOPAZ single crystal diffractometer at the Spallation Neutron Source (SNS), both at ORNL. The results show that the trained network on a few images accurately predicts the sample position on holdout test images. The resulting surrogate model can then be used via feedback-driven adaptive controls to tune the experimental parameters to get the desired beam and sample position.

INTRODUCTION

Neutron scattering experiments probe the structure and dynamics of materials to provide unique insights into physical, chemical, nanostructured, biological and engineering materials science. At present the US Government operates two premier neutron scattering user centers [1]; one at Oak Ridge National Laboratory and one at the NIST Center for Neutron Research. These large scale facilities offer flagship research capabilities to academia and industry that serve a broad and growing user community which necessitates their improved operational efficiency and capacity. The experiments involve collecting data on samples in a neutron beam on highly optimized neutron instruments. The position of the sample in the beam is often critical to the subsequent data analysis and measurements success, however the need to perform sample alignment and realignment during experiments reduces the amount of time spent collecting data. While there have been efforts to improve sample alignment [2] and to automate switching between samples [3, 4], manual intervention from facility beamline scientists or expert users is still necessary. At present optimization of the experimental environment requires a facility beamline scientist or expert user to interpret image data of the sample either through an

optical camera or a neutron camera. A correction is then applied manually based on the data from these images until the sample is aligned in the beam. The automation of this process will result in more efficient and accurate use of neutron facilities and therefore increase the overall quality and reliability of their scientific output. During our studies we have focused on developments for two experimental stations, the HB-2A neutron powder diffractometer and the TOPAZ neutron single crystal diffractometer.

The HB-2A neutron powder diffractometer (as shown in Fig. 1) is located at the High Flux Isotope Reactor at ORNL and is primarily utilized for magnetic structure determination while focusing on experiments at ultra-low temperatures with the options of high external fields or applied pressures. The constant energy neutron beam in a low noise environment and a simple incident beam profile makes HB-2A well suited to a variety of interchangeable environments with minimal calibration required. There are a variety of sample changer options that can allow multiple samples to be loaded at a time. With a focus on weak magnetic signals the sample alignment and beam optimization with adjustable slits and sample stage motors is crucial to reducing unwanted background scattering and to maximise the sample signal. With further optimization of the beamline to include a new detector count rates would increase by over an order of magnitude, resulting in a significant increase in the number of samples being run, further motivating the advancement of automated sample alignment. For more details about the HB-2A instrument and scientific applications see [5].

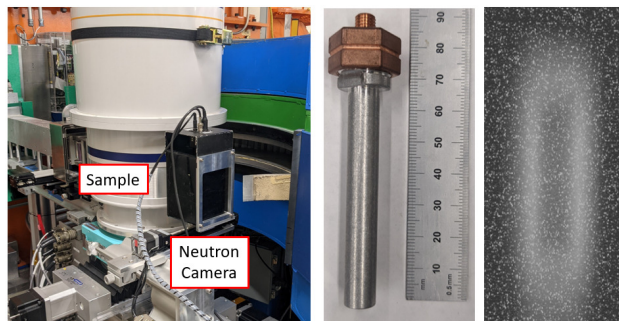


Figure 1: The HB2A powder neutron diffraction instrument. The sample and detector area is shown on the left, with the neutron camera behind the sample. Middle shows a standard sample holder that the powder sample is loaded into, with the scale shown in millimeters. An example of a neutron image is shown on the right, with the powder appearing as a shadow-like image in the white beam.

* diaw@radiasoft.net

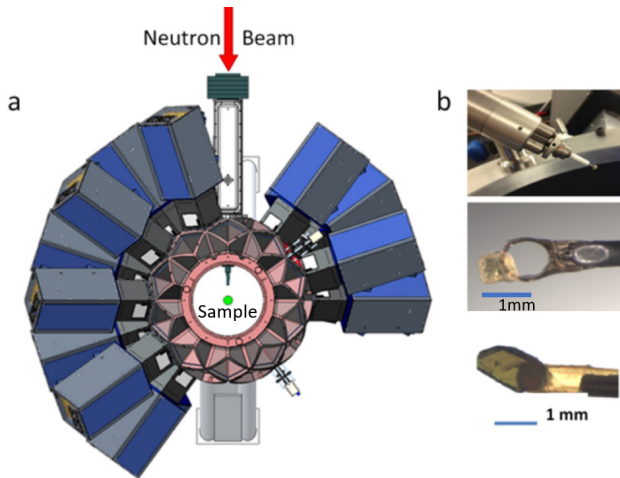


Figure 2: TOPAZ neutron single crystal diffractometer. (a) The sample and detector area is shown as viewed from above the instrument. (b) Top image shows the sample goniometer arm. Samples are loaded on pins and attached to the end of the arm. The middle and bottom images show images of the samples attached to sample mounts.

The TOPAZ neutron single crystal diffractometer (as shown in Fig. 2) is located at the Spallation Neutron Source at ORNL and offers high resolution measurements of crystal structures in small sample volumes. The smallest crystals studied to date in this instrument are 0.065 mm^3 in size. TOPAZ has recently been upgraded to include the installation of a focusing high-flux neutron guide end-section. This enables routine measurements of sub-millimeter crystal samples. TOPAZ is also capable of continuous 3DQ-space mapping for a specific region of reciprocal space volume given a stationary single-crystal sample. This is particularly useful when studying phase transitions as a function of temperature or other external stimuli. TOPAZ possess state of the art data acquisition and reduction tools making it one of the more advanced neutron scattering end stations available for users. These capabilities, however, are under utilized in part due to limited temperature range and manual alignment of the sample in the environment. Improved tools for automatic sample alignment and stabilization promise to increase the throughput of the detector and therefore increase its net scientific output. For more specifics about the TOPAZ diffractometer and other diffractometers at ORNL see [6].

The two neutron beamlines HB-2A and TOPAZ use different methods to image the sample and optimize the alignment. HB-2A uses a neutron camera that is placed in the neutron beam after the powder sample. The sample and any ancillary equipment that are in the neutron beam appear as a shadow in the beam, with the contrast varying depending on the neutron absorbing characteristics of the material. The beam size has a maximum of $20 \text{ mm} \times 60 \text{ mm}$ (Horizontal \times Vertical) and the samples are typically enclosed within a cylindrical can $\sim 60 \text{ mm}$ tall with diameters in the range 4–15 mm. The target sample alignment is to center the sam-

ple in the beam horizontally and vertically, translate to the center of the detector arc to ensure reliable data quality and to mask out any unwanted beam not hitting the sample that would add unwanted background scattering. For the TOPAZ diffractometer, centering of samples in the neutron beam is accomplished via an optical camera. The sample sizes are in the mm to sub mm size, with a beamsize of 2.0–4.0 mm in diameter. The sample shape and dimension are often irregular and can vary significantly between samples. To view the sample a video camera is installed below the sample and individual images or series of images with respect to a marked beam center position are recorded. The sample is aligned remotely using a software algorithm. All associated metadata and beamline configuration data are recorded and associated with the image. This alignment procedure is done both at the start of the experiment when a sample is initially installed and after the sample temperature has changed which results in a non-trivial alteration of the sample position due to thermal expansion/contraction of the sample environment. Temperature changes can occur multiple times per experiment.

Machine learning has recently been of interest for a range of automation tasks in particle accelerators [7, 8] and experimental end stations [9, 10]. Convolutional neural networks are of particular interest due to their ability to efficiently process image data [11, 12]. Here we will detail the prototyping and testing of new machine learning methods for sample alignment and stabilization of samples at neutron scattering beamlines. Our approach employed the use of convolutional neural networks to either relate diagnostic images to a series of machine settings in operational experiments or reconstruct a binary image outlining the sample. These algorithms can then be used during neutron experiments in conjunction with a feedback algorithm to stabilize samples in the beam. This paper provides an overview of our recent efforts to build convolutional neural networks to assist with the automation of sample alignment in neutron beamlines.

METHOD AND RESULTS

We focus on designing an efficient approach to dealing with images of different samples obtained during the neutron-scattering experiment.

First, we consider the HB2A dataset. Figure 1 shows an example of the neutron camera image with the powder appearing as a shadow-like image in the white beam. Our dataset

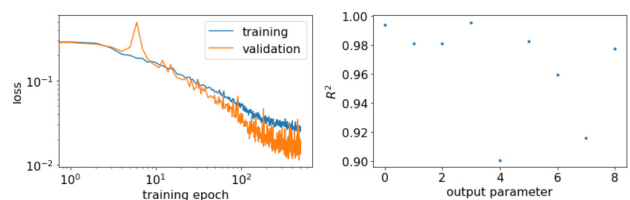


Figure 3: Left: Training an validation loss function at each epoch. Right: the coefficient of determination R^2 for each of the 9 motor parameters.

Content from this work may be used under the terms of the CC BY 3.0 licence (© 2022). Any distribution of this work must maintain attribution to the author(s), title of the work, publisher, and DOI

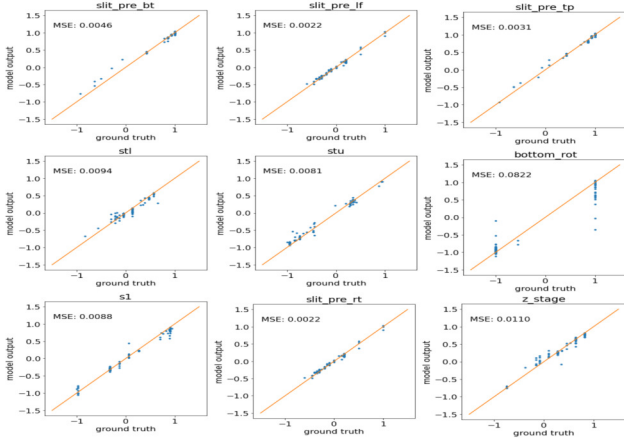


Figure 4: Test of the CNN surrogate performance in the test dataset. Each plot title corresponds to a different instrument motor that can control sample position and beam size. On the x -axis we have the data from the experiment, y -axis represents the model prediction.

consisted of a collection of 530 images sized $480 \times 640 \times 4$ and 9 relevant motor parameters such as smp_stk to selecting the motor position for a sample, stu to translate the sample horizontally in the beam or $slit_pre_tp$ to control the beam size with motorized slits. Our focus was to find a surrogate model that can take a neutron image and predict the motor parameters. This was accomplished using vanilla convolutional neural networks implemented in keras [14]. These structures are well suited for extracting scalar quantities from image data. The CNN consists of a series of 4×4 convolution layers. Each layer comprises three types of operations: convolution, rectified linear units, and batch normalization. A dropout of 0.25 is applied between layers and there is a dense layer (256) after the last convolution. A network was trained to learn the behavior of a dataset; this means fine-tuning each layer’s parameters (weights and biases) to produce a valid model. We employ a conventional formulation based on the minimization of a loss function L with the mean-squared error:

$$L = \frac{1}{n_{\text{batch}}} \sum_{s,t} (\hat{X}_s^t - X_s^t)^2. \quad (1)$$

Here s loops over the training examples, and t runs over training targets. \hat{X}_s^t is the t -th image for example s , and X_s^t is the output of the t -th neuron in the last layer of the network, and where n_{batch} is the batch number. We minimize this output by accelerated gradient descent with Adam optimizer with a learning rate set to $lr = 10^{-4}$ in a series of *epochs*.

Figures 3 and 4 illustrates the network performance. For each motor position, the coefficient of determination $R^2 > 0.9$, indicating that the training approach yields robust surrogate models.

Although we successfully trained a network on the dataset, the inverse problem of predicting a sample position from the CNN model using the machine setting parameters did not yield good results. Much of this is related to the degenerate

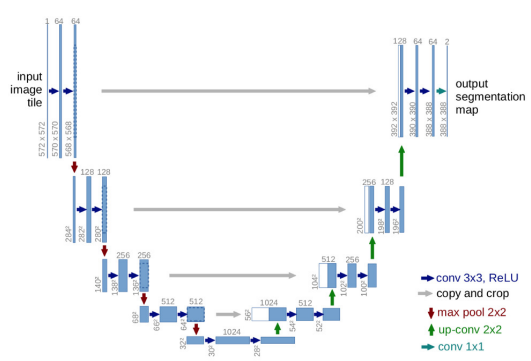


Figure 5: The proposed U-net architecture uses a contraction and an expansion paths. The blue boxes represent multi-channel feature map while the white boxes are their copies. The gray arrows correspond to the operations from left to right. This figure was taken from Ref. [13].

nature of the system. This limits our ability to provide a feed-forward adjustment to the motors based on a neural network model. An alternative approach is to identify the sample position from the image and use feedback on the motors to position the sample. This sample identification approach was applied to the Topaz dataset using a slightly different architecture.

For the Topaz data, our problem is as follows: Given an image, localize sample position in the image and return the center of the mass of the sample. To do so, we trained a convolution neural network based on the segmentation algorithm 2D-U-net [13]. The U-net architecture shown in Fig. 5 consists of contracting and expansive paths and overall has 23 convolutional layers. For the contracting layer, a vector input y is passed to two 3×3 convolutions, each followed by an activation unit, and produces a vector of activations, y' , via

$$y' = f(Wy + b), \quad (2)$$

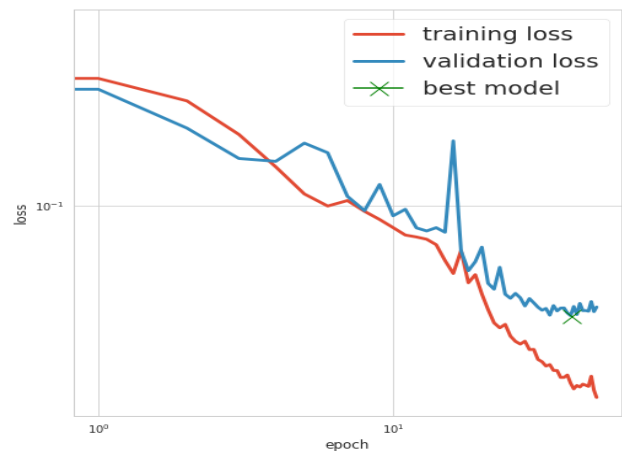


Figure 6: Learning curve. Training and validation loss at each *epoch*.

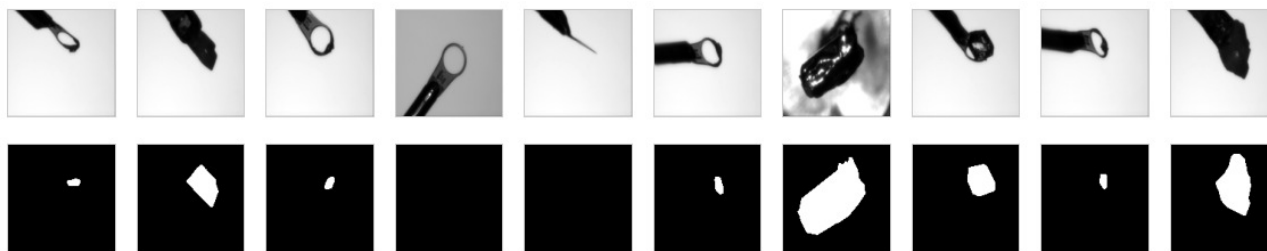


Figure 7: Examples images obtained from the experiment. The lower plots show binary image masks created around the sample. For images with no sample the mask is empty.

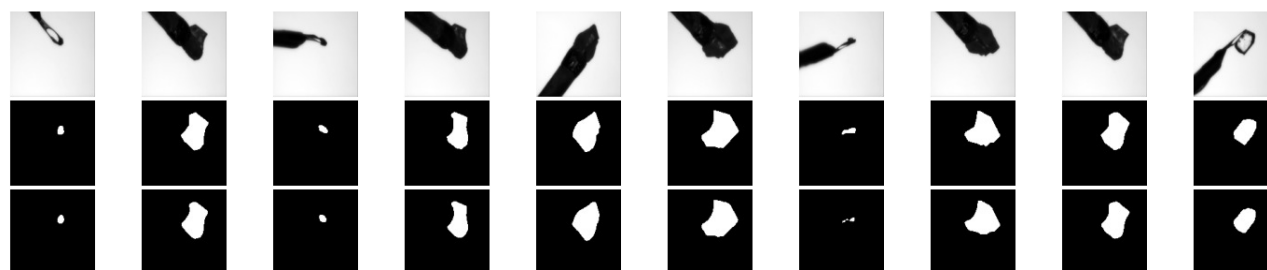


Figure 8: Test model performance for some random images in the test dataset. Top row are the test image (ground truth), middle row: the test image label, and bottom row are the predicted test binary by the U-net algorithm. The predicted test image is visually identical to the ground truth.

where W is a weight matrix, b is a bias vector, and f is an activation function. We choose the rectified linear unit (ReLU) function $f(s) = \max(0, s)$. Then, we introduce a downsampling layer consisting of 2×2 max pooling operation with stride 2. The downsampling factor was set 2 at each step while the number of feature channels doubles. For the expansive path, we have an upsampling operator of the feature map. A 2×2 convolution is employed to reduce the number of feature channels and two 3×3 convolutions. After the last convolution layer, we applied a 1×1 convolution to map each 64-component feature vector to produce the desired clean image.

Our training dataset is composed of images and the corresponding masks (binary), where each image of size 964×1292 has either a sample or no sample, as shown in Fig. 7. Because these images are extremely large, we resized them to 128×128 before applying them to the network. Although this procedure may introduce artifacts in the sample images, it did not seem to impact the result of the training. The dataset consists of 611 images, and it was obtained by randomly varying the parameter settings of the optical camera images from the TOPAZ single crystal diffractometer. All model evaluation was carried out using a hold-out 20% validation set, which contains no overlap with the training set. We used a formulation based on the cross-entropy loss function. This latter is minimized by accelerated gradient descent with the Adam optimizer in a series of epochs, that is, passes over the entire training dataset, using a learning rate of 10^{-3} and batches of size $n_{\text{batch}} = 32$. A patience-based learning scheduler is used to stop the training and revert to the last best network if the validation loss does not

improve over $n_{\text{patience}} = 10$ epochs, with a global termination of $n_{\text{epochs}} = 500$ at maximum. Figure 6 illustrates the training and validation loss error. The network terminates within few epochs (~ 50).

Finally, Fig. 8 shows random samples from the ground truth data, their labels, and corresponding predictions obtained using our surrogate model, demonstrating that the u-net approach captures details very accurately across the sample types.

CONCLUSION

Machine learning tools are promising for the increased automation of neutron beamlines. We have shown the ability for convolutional neural networks to predict motor positions from images in the HB-2A beamline and to contour the sample for optical images collected from the TOPAZ beamline. Using the output of the U-net architecture we can compute the center of mass of the sample and hand that off to the motor controllers in order to maintain sample alignment during the experiment.

ACKNOWLEDGMENTS

This work was supported by the DOE Office of Science Office of Basic Energy Science SBIR award number DE-SC0021555. This research used resources at the High Flux Isotope Reactor and Spallation Neutron Source, a DOE Office of Science User Facility operated by the Oak Ridge National Laboratory.

REFERENCES

- [1] DoE, “Neutron Scattering Facilities: U.S. DOE Office of Science (SC)”, July 2019.
- [2] J. A. O’Toole, “Advances in neutron science instrumentation at the Los Alamos Neutron Science Center (LANSCE)”, *IEEE Nuclear Science Symposium Conference Record*. vol. 1, pp. 627–632, 2007.
- [3] H. M. Reiche and S. C. Vogel, “A versatile automated sample changer for texture measurements on the high pressure-preferred orientation neutron diffractometer”, *Review of Scientific Instruments*, vol. 81, no. 9, p. 093302, 2010. doi: 10.1063/1.3485035
- [4] J. E. Rix *et al.*, “Automated sample exchange and tracking system for neutron research at cryogenic temperatures”, *Review of Scientific Instruments*, vol. 78, no. 1, p. 013907, 2007. <https://doi.org/10.1063/1.2426878>
- [5] S. Calder *et al.*, “A suite-level review of the neutron powder diffraction instruments at Oak Ridge National Laboratory”, *Review of Scientific Instruments*, vol. 89, no. 9, p. 092701, 2018. doi: 10.1063/1.5033906
- [6] L. Coates *et al.*, “A suite-level review of the neutron single-crystal diffraction instruments at Oak Ridge National Laboratory”, *Review of Scientific Instruments* vol. 89, no. 9, p. 092802, 2018. doi: 10.1063/1.5030896
- [7] A. L. Edelen *et al.*, “Neural Networks for Modeling and Control of Particle Accelerators”, *IEEE Transactions on Nuclear Science*, vol. 63, no. 2, pp. 878–897, Apr. 2016. issn: 0018-9499.
- [8] A. L. Edelen *et al.*, “Opportunities in Machine Learning for Particle Accelerators”, 2018. arXiv:1811.03172
- [9] S. C. Leemann *et al.*, “Demonstration of Machine Learning-Based Model-Independent Stabilization of Source Properties in Synchrotron Light Sources”, *Phys. Rev. Lett.*, vol. 123, p. 194801, 19 Nov. 2019.
- [10] B. Nash *et al.*, “Reduced model representation of x-ray transport suitable for beamline control”, in *Proc. SPIE 11493, Advances in Computational Methods for X-Ray Optics V, (SPIE Proceedings Vol. 11493)*, 21 August 2020, pp. 53–61. doi:10.1117/12.2568187
- [11] R. Venkatesan and B. Li., *Convolutional Neural Networks in Visual Computing: A Concise Guide*, CRC Press, 2018.
- [12] B. Nash *et al.*, *Convolutional Neural Networks in Python: Beginner’s Guide to Convolutional Neural Networks in Python*, CreateSpace Independent Publishing Platform, 2018.
- [13] O. Ronneberger *et al.*, “U-Net: Convolutional Networks for Biomedical Image Segmentation”, 2015. arXiv:1505.04597
- [14] F. Chollet *et al.*, “Keras”, 2015. <https://github.com/fchollet/keras>